stellarator news

Published by Fusion Energy Division, Oak Ridge National Laboratory
Building 9201-2 P.O. Box 2009 Oak Ridge, TN 37831-8071, USA

Editor: James A. Rome Issue 87 May 2003
E-Mail: jar@ornl.gov Phone (865) 574-1306
On the Web at *http://www.ornl.gov/fed/stelnews*

Experiments with dual heavy ion beam probes in CHS

The structure and dynamics of the radial electric field (E_r) is an important issue for toroidal plasma research since the radial electric field structure should be closely related to the transport barrier formation. In the Compact Helical System (CHS), a heavy ion beam probe (HIBP) has revealed a number of interesting phenomena associated with E_r, such as bifurcation, self-organized oscillation (or electric pulsation), internal transport barrier formation, and so on [1]. A second HIBP has been constructed and installed in order to further understand unsolved physics problems. Recently the initial results have been obtained.

The two HIBPs (maximum beam energy: 200 keV) are located at toroidal positions 90 degrees apart. Because the topologies of the two diagnostic systems and their installations are identical, the topologies of measurements such as measurable areas and scanning traces are also identical when the torus is rotated by 90 degrees because CHS has eight field periods (N = 8).

Each HIBP can be operated in two different modes. In the first, radial position is scanned by sweeping the beam trajectory continuously to obtain the potential profile (scanning mode). Time evolution of the potential profile can be measured every few milliseconds at the fastest sweep speed. The second mode fixes the observation point in order to investigate dynamics or fluctuation of the plasma (fixed-point mode). In this mode, the temporal resolution is up to a frequency of 250 kHz at present.

The first measurements were performed in a low-density plasma with combined heating by neutral beam injection (NBI) and electron cyclotron resonant heating (ECRH). The discharges are performed in a magnetic configuration whose axis is located at R_{ax} = 0.921 cm with a field strength of 0.88 T. The electron cyclotron resonance is exactly on the magnetic axis at the gyrotron frequency, 53.2 GHz. The necessary beam energy to observe this configuration is ~70 keV when a cesium beam is used. After ECRH is turned on, the density starts to decrease and relaxes to the steady-state value of $n_e \sim 0.5 \times 10^{13}$ cm^{-3}. In the steady state, the potential signal shows pulsation with a quasi-coherent frequency of ~750 Hz. After the NBI is turned off, the pulsation amplitude disappears in ~10 ms. Similarly, a high-frequency mode develops after the ECRH is launched. In this combined heating phase, the high-frequency mode is continuously observed in the potential fluctuation of the HIBP, and it disappears ~10 ms after the NBI is turned off.

The potential waveforms from both HIBPs show coherent pulsation behavior. Figure 1(a) represents the waveforms of the HIBPs, where one is operated with the observation point fixed at the plasma center and the other is in scanning mode; the triangular waveform in the figure indicates the observation point as a function of time. As the potential is scanned, several sharp dips are found, synchronized with a corresponding potential pulse at the central potential. Utilizing the good correlation, the upper state profile of bifurcation can be deduced by removing the effects of pulse-like events. The lower state profile can also be approximately constructed by picking up potential values at the scanning radius when the pulse at the plasma center

In this issue . . .

reaches minimum values. The bifurcated potential profiles are shown in Fig. 1(b).

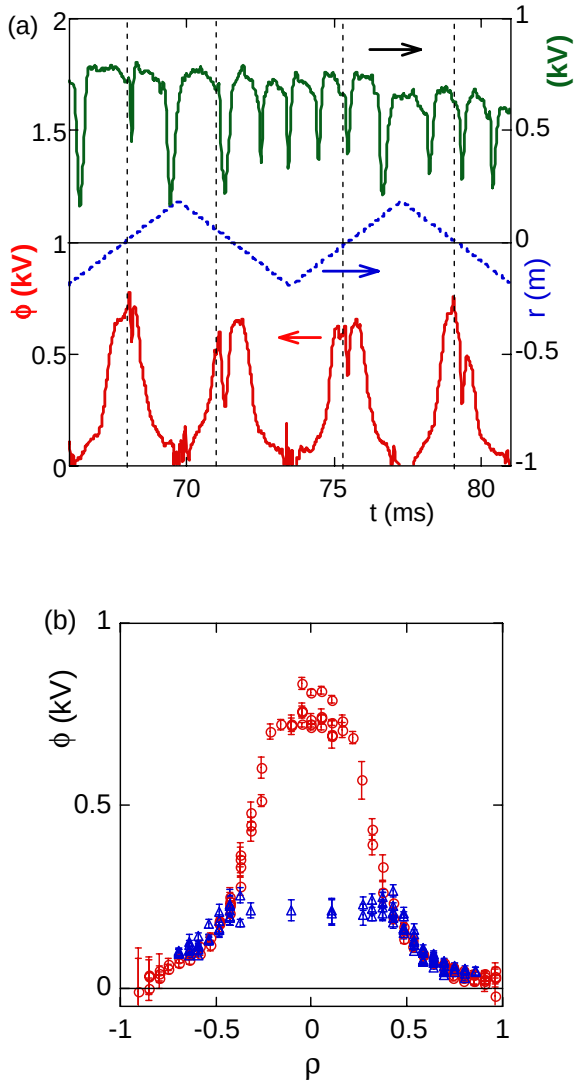

Fig. 1. (a) Potential pulsation waveforms. The first HIBP is in radial scan mode, while the observation point of the second HIBP is fixed at the center. The dashed line shows the observation radius for the scanning. (b) Potential profiles after the effects of pulse-like events are removed. The images of two bifurcated states during pulsation emerge.

The propagation in the potential pulse can be determined by operating both HIBPs in fixed-point mode, which is accomplished by moving the observation point of one HIBP system with the other observation point fixed as a reference. The comparison reveals that the potential pulse propagates outward, with the negative pulse inside changing its sign to become a positive pulse outside the normalized radius of $r/a \sim 0.5$. Apart from the core behavior, examining the relationship between the plasma core and the edge region reveals an intriguing situation. The detected beam intensity from the region around $r/a \sim 0.7$–0.8 shows quite large changes (more than 50%) that appear to be synchronized with the central potential pulsation. The time scale of these changes is as fast as the transition time of the central potential. From upper to lower state, the transition time is ~50 μs , that of the opposite is ~80 μs . This correlation could be a manifestation of the nonlocal nature of the phenomenon, providing an interesting future subject for future investigation.

In the same discharges, a high-frequency (~180-kHz) fluctuation has been found in both density and potential signals of the HIBP. In particular, a coherent mode can be clearly identified in the potential fluctuation. The fluctuation has been found to correlate well with the magnetic field pick-up signals (Mirnov coils). The fluctuation appears in the potential fluctuation spectra as a clear peak with a bandwidth of ~10 kHz. The amplitude increases with radius in this range. The potential fluctuations measured by the HIBP at this frequency show quite high coherence of ~0.7 at the same normalized radius, while the density fluctuations do not show any significant coherence.

The dual HIBPs have just begun to work in CHS. In addition, we are developing a new ion source to increase beam intensity by more than 10 times. This improvement will bring information on potential fluctuation due to microinstabilities as well as density fluctuations. Future experiments promise to yield valuable observations to develop plasma physics and fusion research.

A. Fujisawa
National Institute for Fusion Science
Oroshi-cho, Toki, Japan 509-5292
E-mail: fujisawa@nifs.ac.jp

References

[1] A. Fujisawa et al., Phys. Plasmas **7,** 4152 (2000).

U.S./Japan JIFT workshop on "Theoretical Considerations on Helical Plasmas"

A U.S./Japan Joint Institute for Fusion Theory (JIFT) workshop, "Theoretical Considerations on Helical Plasmas" was held in Princeton, New Jersey, USA, on 18–20 November 2002. Sixteen talks were presented. The talks focused mostly on currently operating stellarators, LHD, Heliotron-J, W7-AS, and HSX, and on future experiments such as QPS, W7-X, and NCSX. We present below a synopsis of the talks in alphabetical order by first author. The viewgraphs from these talks appear on the Web at

http://www.pppl.gov/ncsx/Scientificconf/JIFT/JIFT.html

Don Monticello and Nori Nakajima
Conference Organizers

Synopsis of talks

Determination of perturbations that cause magnetic islands using a δW code

A. Boozer and C. Nührenberg

A method is presented to calculate the width of islands produced by external perturbations of the surface of a equilibrium plasma. The procedure uses an ideal MHD δW code to calculate the jump in the resonant displacement at the rational surfaces. This displacement is then related to the width of islands that would appear if no singular currents appeared on the rational surfaces. An application of this method is made to W7-X using the CAS-3D code.

Reactor studies for the LHD and the MHH2

P. R. Garabedian

The NSTAB and TRAN codes are validated by comparison with experimental results from the LHD experiment at NIFS. NSTAB predicts stability of LHD at betas of 3.2% in agreement with the experiments and in disagreement with the ballooning estimates. Energy confinement times from TRAN are also in agreement with experimental results.

This agreement with experiment lends credibility to the application of the NSTAB and TRAN codes to a reactor based on the MHH2 concept. It is found that the reactor is stable to betas of 4% and has robust magnetic surfaces. In addition the confinement properties are more than sufficient for a reactor.

Implications of field line tracing for power and particle handling in NCSX

A. Grossman et al.

Using the MFBE and free boundary VMEC codes the nature of the magnetic field outside the last closed magnetic surface is investigated in NCSX. It is found that configurations with healed surfaces inside the plasma have longer connection lengths than unhealed configurations. A simple two point model temperature calculation shows that the connection lengths in NCSX are long enough to provide suitable divertor operation.

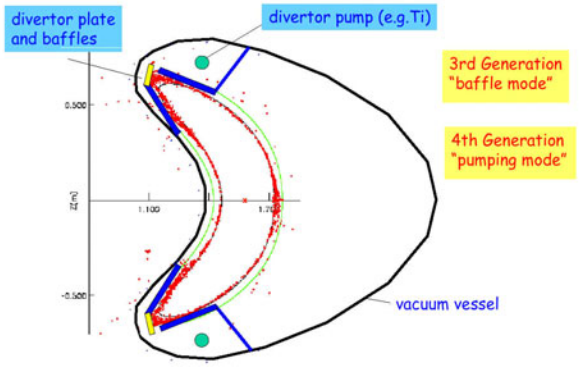

NCSX divertor model with field line traces

Ideal MHD ballooning stability in three-dimensional equilibria

C. C. Hegna, S. R. Hudson, and R. Torasso

A technique is presented that allows a characterization of the regions of stability to ballooning for stellarators. The method involves creating sets of equilibria by perturbing an equilibrium locally to produce a family of new equilibra. Results of the stability study of these perturbed equilibria show a sensitivity to symmetry-breaking terms in the local shear, a deterioration or elimination of second stability regimes, and a dependence on field lines on each flux surface.

Suppression of magnetic islands in stellarator equilibrium calculations

S. R. Hudson et al.

A description of the design process for the NCSX stellarator coils is described. The coils are first designed using VMEC and STELLOPT and various design metrics, such as transport, stability, and coil engineering constraints. The final design is then handed to the PIES code, which reoptimizes the coils using the same constrains as in the VMEC-STELLOPT stage plus the constraint of good flux surfaces. The results of the iterative solution of this problem are presented, showing good and robust flux surfaces

.

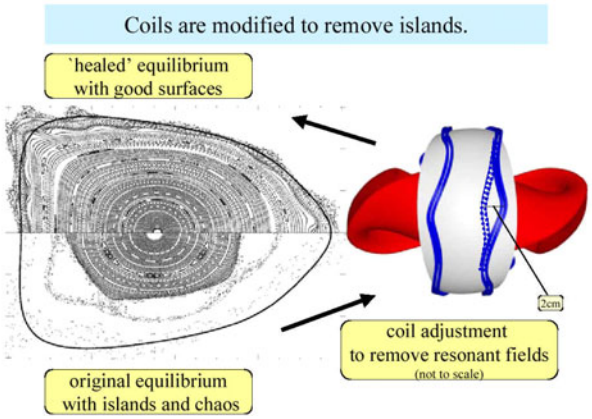

Island healing in NCSX.

Nonlinear MHD analysis for LHD plasmas

K. Ichiguchi et al.

Nonlinear development of interchange modes in LHD is investigated for experimentally relevant MHD equilibria. For low-beta equilibria, the growth rates of the excited modes are so small and the number of unstable modes is so low that saturation is brought about by the local flattening of the pressure profile around mode rational surfaces. However, for high-beta equilibria, the growth rates of the excited modes and their number are so large that direct interaction of neighboring unstable modes leads to a bursting activity and global reduction of the core pressure. Moreover, it is shown that along the path to high-beta equilibria, the MHD activity changes significantly.

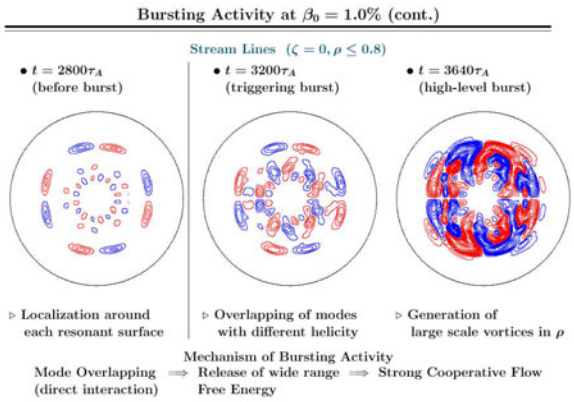

Bursting activity in an LHD-like plasma.

Fluid simulation on pellet ablation

R. Ishizaki, N. Nakajima, and P. B. Parks

A new code using a CIP (cubic-interpolated pseudoparticle) scheme is developed to investigate the ablation process of pellets. The code includes various atomic processes and can treat the pellets from the solid phase to the gas phase continuously, without any boundary condition between different phases. Simulated are the existence of a stationary shock wave driven by the energy loss due to ionization and the deformation of the pellet by a nonuniform ablation pressure in a two-dimensional system. Pellet deformation shortens the pellet lifetime.

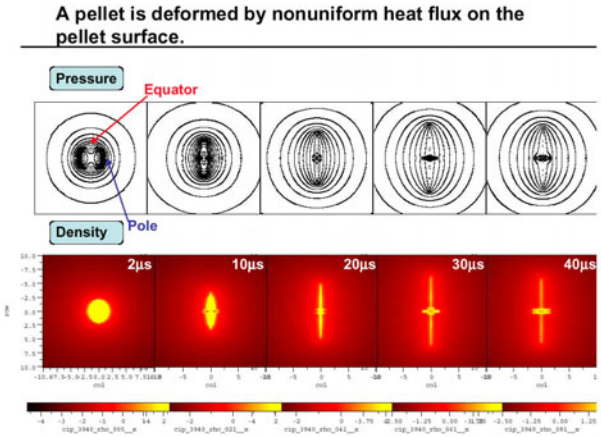

Computational study of LHD equilibrium

R. Kanno et al.

LHD has a coil system used to create an (m,n) = (1,1) magnetic island externally, which will be used as an island divertor. The HINT code has been modified to treat MHD equilibria with an (m,n) = (1,1) magnetic island. A new scheme has been implemented in the evolution of the pressure in order to reduce the convergence error near the island edge, where the pressure gradient changes significantly. The added diffusion process works well, and allows a well-converged MHD equilibrium with an (m,n) = (1,1) magnetic island to be obtained.

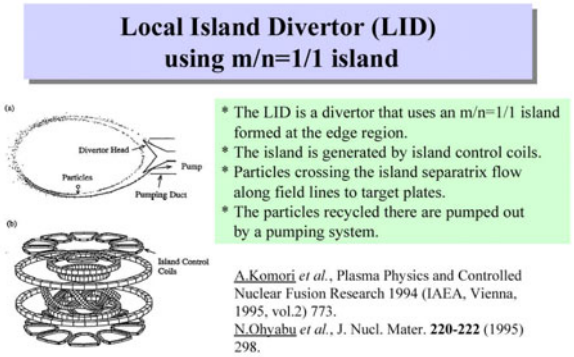

Delta-function currents in VMEC

D. Monticello, M. Isaev, A. Reiman, A. Subbotin, M. Mikkhailov, and S. Hirshman

It is shown that fixed boundary VMEC does include delta-function currents in its calculation of the equilibrium ***B*** field, but it requires a large number of radial zones, and poloidal and toroidal harmonics to observe them. This observation is true even in zero-current, zero-beta cases. This result could potentially be used in VMEC applications to design coils for stellarator equilibria that have good surfaces. However, the convergence of free boundary VMEC at these large numbers of radial zones and harmonics remains an issue.

Exploration of transport-optimized stellarator configuration space

H. E. Mynick and N. Pomphrey

An extension of earlier work on classification of various quasi-axisymmetric designs is presented. The new work now includes other transport-optimized configurations such quasi-omnigenious, quasi-poloidal, and quasi-helical designs. Various seed configurations such as LI383 from NCSX, QPS3a from QPS, and HSX3a from HSX are used to initialize the space of performance metrics. The results show that there are only a modest number of basins and that therefore distinct classifications of transport-optimized configurations exist.

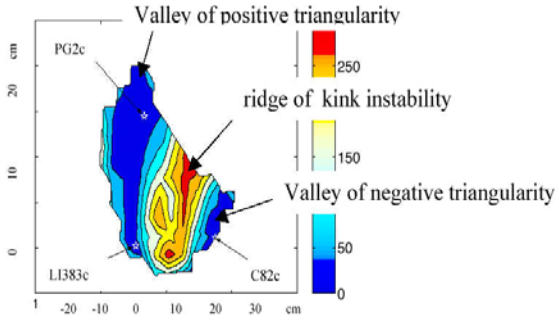

Configuration space of QA stellarators.

Shear Alfvén spectrum in helical systems: continuum and point spectra

N. Nakajima

Shear Alfvén spectra around the HAE (helicity-induced shear Alfvén eigenmodes) frequency range are essentially different from those around the TAE (toroidicity-induced shear Alfvén eigenmodes) frequency range. In the TAE frequency range, spectral gaps are created by axisymmetric equilibrium components, so that from analogy with the Mathieu equation those gaps that are well separated by the continuum have no point spectra inside the gaps. It is found, however, that in the HAE frequency range, neighboring spectral gaps are created by equilibrium Fourier components without any symmetric relation to each other, so that the spectral gaps are not well separated by the continua, and hence point spectra may exist in those gaps.

MHD equilibrium and pressure driven instabilities in $\ell = 1$ heliotron plasmas

Y. Nakamura et al.

MHD equilibria and linearized ideal MHD stability in Heliotron J are discussed. Improved schemes applied to the PIES and HINT codes are presented which help resolve difficulties in Heliotron J free boundary MHD equilibria with strong boundary shaping and large magnetic islands. For equilibria with good nested flux surfaces, local and global mode analyses are performed. It is shown that stellarator-like magnetic shear is stabilizing to helical ballooning modes in a low shear system. It is also shown that the theoretical prediction of the bootstrap current is consistent with the experimental results.

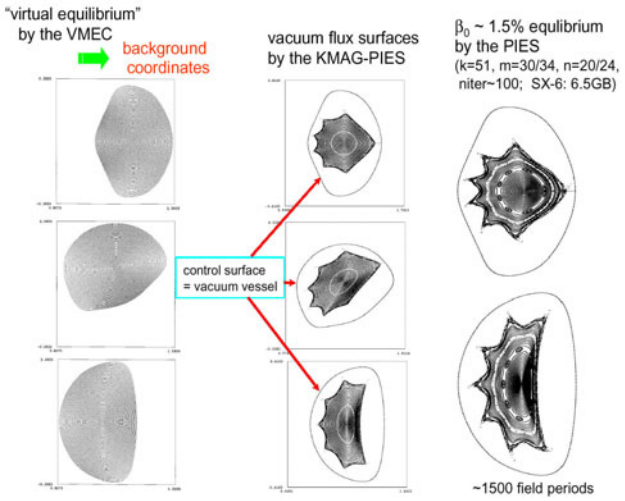

Equilibrium calculation with the KMAG_PIES code.

Magnetic islands in NCSX and their suppression by plasma flow

A. Reiman, et. al.

The strong ambipolar flow predicted to exist in the NCSX device is shown to reduce the vulnerability of the device to perturbing resonant magnetic fields. A comparison with a DIII-D experimental shot, in which most of the key parameters are approximately equal to those of NCSX, is presented.

Transport and energetic particle confinement issues for compact stellarators

D. A. Spong

The flexibility of the QPS stellarator being designed at ORNL is presented. Using codes such as NEO, DKES, BOOTSJ, and DELTA5D, the flexibility in the design is illustrated for transport, bootstrap current, and global ion confinement.

Alpha particle confinement is shown to improve dramatically with increasing beta due to the closing of |B| contours. Other energetic particle issues, such as fast ion driven Alfvén instabilities, are discussed from the point of view of a low-aspect-ratio device causing more closely coupled toroidal modes and stronger equilibrium mode coupling.

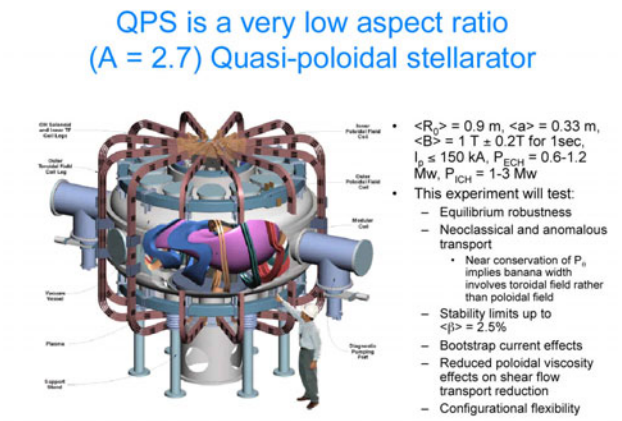

Nonlinear MHD and energetic particle modes in stellarators

H. R. Strauss, L. E. Sugiyama, G. Y. Fu, W. Park, and J. Breslau

Application of the M3D code to the NCSX stellarator shows that resistive ballooning modes occur much below the ideal ballooning limit and there is no stabilization of these modes at small resistivity from the Glasser effect because NCSX is unstable to the resistive interchange mode. However, stabilization of these resistive modes was found for realistic values of the Hall parameter using the two-fluid version of M3D. In fact, the two-fluid effects can stabilize the ideal modes, significantly increasing the beta limit.

Hot particle effects were also investigated and shown to be more stable than in a corresponding tokamak.

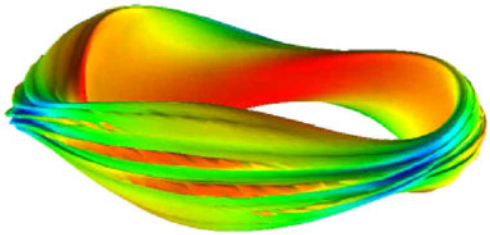

Ballooning mode in NCSX stellarator using M3D.

Application of the HINT code to Heliotron J plasmas

Y. Suzuki et al.

Heliotron J is a device with low magnetic shear in the vacuum configuration, whose boundary is determined by magnetic islands. Thus, for example, a change in the rotational transform caused by the Shafranov shift leads to a change of the boundary shape. To investigate the properties of the MHD equilibria, a modified HINT code is used, where new numerical techniques are introduced. The most significant of these is a technique to reduce the computational time required to effect the relaxation of the pressure. Here, field line tracing is combined with linear interpolation of the pressure profile. In spite of a fairly large stochastic region, good numerical convergence is attained.

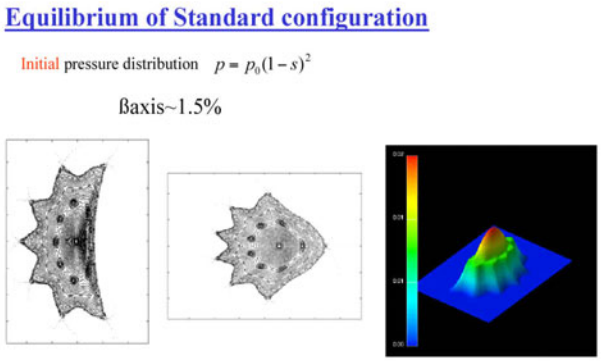

Heliotron J equilibrium with the HINT code.

Abstracts

High-resolution ruby laser Thomson scattering diagnostic for the W7-AS stellarator

Rev. Sci. Instrum. **74** (March 2003) 1679

After reconstruction, the ruby Thomson scattering diagnostic for the W7-AS stellarator is now in operation to again cover the complete plasma cross section (420 mm). The former photomultiplier-based polychromator system has been replaced by two individual Littrow-type polychromator setups (focal length 50 cm), using intensified charge coupled device cameras for light detection. A single-pulse ruby laser with high pulse energy is used as a light source. The geometry is shown in Fig. 1.

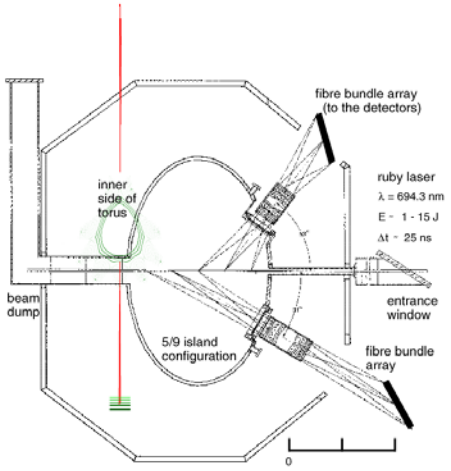

Fig. 1. Scattering geometry and detection optics of W7-AS ruby Thomson scattering diagnostic. The plasma contour represents a 5/9 island configuration.

The light scattered by the plasma electrons is imaged upon a set of 45 fiber bundles. 30 bundles provide a high spatial resolution of 4 mm at the inner edge of the plasma. The remaining part of the view chord is observed with a spatial resolution of 20 mm. At the output, the fiber bundles form the entrance slits of the Littrow-type spectrometers. The spectral resolution of the edge spectrometer can be modified by exchanging the diffraction grating. Depending on the installed diffraction grating (600 or 1800 lines/mm) a total wavelength range of 80 nm (suitable for plasma edge investigations) or 320 nm (suitable for gradient investigations) can be surveyed.

The spectral, geometrical, and intensity calibrations of the presented diagnostic setup can be done in situ by means of a neon spectral lamp and a calibrated tungsten strip lamp. The absolute sensitivity calibration for the system is achieved using either Raman (at 723.8 nm) or Rayleigh (at laser wavelength) scattering as hydrogen gas is introduced into the vacuum vessel (up to 100 mbar). Examples of electron density and temperature profiles measured under different plasma conditions are presented.

J. P. Knauer, E. Pasch, G. Kühner, and the W7-AS Team

Turbulence at the transition to the high density H-mode in Wendelstein 7-AS plasmas

Nucl. Fusion **43** (January 2003) 40–48
http://stacks.iop.org/NF/43/40

Recently a new improved confinement regime was found in the Wendelstein 7-AS (W7-AS) stellarator. The discovery of this high density high confinement mode (HDH-mode) was facilitated by the installation of divertor modules. In this paper, measurements of short wavelength density fluctuations in the HDH-mode using collective scattering of infrared light are presented. These measurements will be contrasted to fluctuations during normal confinement operation (NC-mode). The autopower spectra of the measurements show a consistent increase of the fluctuation level associated with the transition from NC- to HDH-mode as shown in Fig. 2.

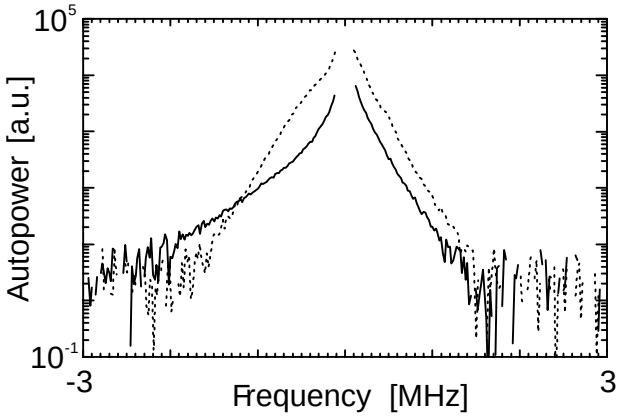

Fig. 2. Comparison of scattered autopower at an electron density fluctuation wave number component perpendicular to the magnetic field of 20 cm^{-1} between normal confinement (solid) and HDH-mode (dotted). Positive and negative frequencies correspond to opposite propagation directions. The scattered power is lower in normal confinement except for frequencies above 1 MHz for inward movement along the major radius.

Correlation calculations on a 20 μs time scale between magnetic and density fluctuations lead to the result that the fluctuations are correlated in NC but not in HDH-mode.

Finally, a comparative analysis between the enhanced D_α H-mode (EDA H-mode) found in the Alcator C-Mod tokamak and the HDH-mode in W7-AS is carried out.

N. P. Basse, S. Zoletnik, S. Bäumel, M. Endler, M. Hirsch, K. McCormick, A. Werner and W7-AS Team.

Charge-exchange spectroscopy at the W7-AS stellarator employing a high-energy Li beam

Plasma Phys. Controlled Fusion, **45** (January 2003) 53.
http://stacks.iop.org/PPCF/45/53

Combined measurements of ion density, temperature and poloidal rotation of impurity ions have been carried out in the gradient region of the Wendelstein 7-AS (W7-AS) plasma, employing charge-exchange spectroscopy with the high energy neutral Li beam and C^{6+} / C^{5+} ions.

The present state of the experimental technique is described. Results are obtained in discharges with high central ion temperatures of 1.3 keV, central electron densities of 7×10^{19} m^{-3}. Under these conditions the diagnostic covers a region of about 7 cm in radial extent, corresponding to ion temperatures (Fig. 3) between 50 and 800 eV. Poloidal rotation velocities (Fig. 4) up to 35 ± 2.5 km/s were measured in a narrow shear layer at the plasma edge.

The contribution of ion diamagnetic and $\boldsymbol{E} \times \boldsymbol{B}$ drift is discussed. The radial electric field is derived from a simplified radial force balance equation.

H. Ehmler, J. Baldzuhn, K. McCormick, A. Kreter, T. Klinger, and the W7-AS Team
E-mail: ehmler@ipp.mpg.de

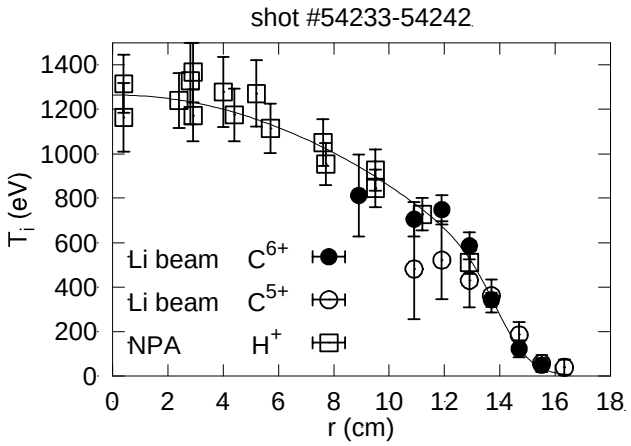

Fig. 3. Radial profiles of ion temperature as obtained by the Li beam diagnostic neutral particle analyzer (NPA) as a function of effective plasma radius.

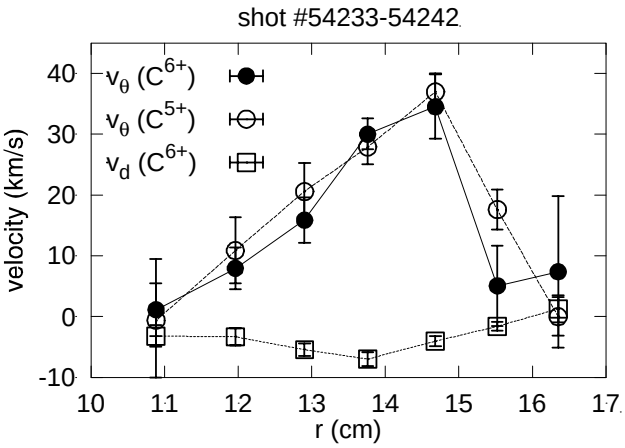

Fig. 4. Poloidal rotation velocity v_θ and diamagnetic velocity v_d measured by the Li beam for C^{6+} and C^{5+} ions.